Journal of *Marine Science and Engineering*

MDPI

Article

Intelligent Model for Dynamic Shear Modulus and Damping Ratio of Undisturbed Marine Clay Based on Back-Propagation Neural Network

Qi Wu [1,2], Zifan Wang [1], You Qin [1] and Wenbao Yang [1,3,*]

[1] Institute of Geotechnical Engineering, Nanjing Tech University, Nanjing 210009, China
[2] Faculty of Architecture, Civil and Transportation Engineering, Beijing University of Technology, Beijing 100124, China
[3] School of Civil Engineering, Chongqing University, Chongqing 400045, China
* Correspondence: yangwenbao1994@163.com

Abstract: In this study, a series of resonant-column experiments were conducted on marine clays from Bohai Bay and Hangzhou Bay, China. The characteristics of the dynamic shear modulus (G) and damping ratio (D) of these marine clays were examined. It was found that G and D not only vary with shear strain (γ), but they also have a strong connection with soil depth (H) (reflected by the mean effective confining pressure (σ_m) in the laboratory test conditions). With increasing H (σ_m) and fixed γ, the value of G gradually increases; conversely, the value of D gradually decreases, and this is accompanied by the weakening of the decay or growth rate. An intelligent model based on a back-propagation neural network (BPNN) was developed for the calculation of these parameters. Compared with existing function models, the proposed intelligent model avoids the forward propagation of data errors and the need for human intervention regarding the fitting parameters. The model can accurately predict the G and D characteristics of marine clays at different H (σ_m) and the corresponding γ. The prediction accuracy is universal and does not strictly depend on the number of neurons in the hidden layer of the neural network.

Keywords: marine clay; dynamic shear modulus; damping ratio; mean effective confining pressure; intelligent model; back-propagation neural network

Citation: Wu, Q.; Wang, Z.; Qin, Y.; Yang, W. Intelligent Model for Dynamic Shear Modulus and Damping Ratio of Undisturbed Marine Clay Based on Back-Propagation Neural Network. *J. Mar. Sci. Eng.* **2023**, *11*, 249. https://doi.org/10.3390/jmse11020249

Academic Editor: Hem Bahadur Motra

Received: 21 December 2022
Revised: 13 January 2023
Accepted: 17 January 2023
Published: 19 January 2023

1. Introduction

Recently, the increasing exploitation of marine resources has led to an increasing number of engineering construction projects in marine and coastal areas, including tunnels, bridges, offshore wind power facilities, and offshore oil platforms. In comparison to general engineering, marine engineering structures suffer from a greater number of technical issues concerning seismic resistance. Marine soil is the supporting layer for marine engineering, and it is also the transfer medium for seismic waves; its dynamic properties, thus, have a direct effect on the seismic responses of marine engineering structures.

The dynamic behavior of soil is principally characterized by nonlinearity and hysteresis in the dynamic stress–strain relationship. This is usually defined using two important parameters: the dynamic shear modulus G and the damping ratio D. Many previous experimental and numerical investigations have been conducted to describe the variations of G and D with the shear strain γ in different soils. The factors affecting these parameters, such as the mean effective confining pressure σ_m, over-consolidation ratio, plasticity index (PI), specimen size, stress anisotropy, saturation condition, grain size, mixture, and void ratio (e), have also been examined [1–11]. However, due to the technical complexity and high expense of overseas drilling, research into the variation characteristics of G and D in marine soil—particularly in cohesive marine clay—has so far been limited and inadequate.

Koutsoftas and Fisher [12] studied the effect of stress history on marine clay by means of resonant column (RC) and cyclic triaxial tests. Vrettos and Savidis [13] systematically

investigated the effects of e, PI, and σ_m on marine clays in Greece by means of RC tests. Sun et al. [14,15] analyzed the effects of σ_m, PI, and the experimental apparatus on marine clay from China's Qiongzhou Strait. Banerjee and Balaji [16] investigated the effects of anisotropic consolidation (stress ratio K_c) on Chennai marine clay using a series of cyclic triaxial and RC tests. Senapati et al. [17] also used a series of cyclic triaxial and RC tests to investigate the influence of frequency on marine clay from the Ennore coast of India's Tamil Nadu saturated with various pore fluids. Li et al. [18] explored the influence of σ_m on several types of marine soil containing marine clay in China's Yellow Sea using dynamic triaxial testing.

On the other hand, geotechnical and earthquake engineering practice requires the establishment of empirical relationships that represent dynamic shear modulus degradation versus shear strain (G/G_{max}–γ) and damping ratio growth versus shear strain (D–γ). To this end, numerous researchers have analyzed this problem and proposed various functions applicable to their data. Hardin and Drnevich [19] published the first function model describing the nonlinear and hysteretic behavior of soil. They proposed a hyperbolic model to reflect the shear modulus degradation (G/G_{max}–γ), as well as an approximate model for material damping growth (D–γ), which is related to G/G_{max}. Much subsequent research was influenced by this work, and different considerations have been introduced to perfect their equations [20–24]. A summary of the representative function forms used to determine the shear modulus degradation versus shear strain γ (G/G_{max}–γ) and the damping growth versus shear strain γ (D–γ) are presented in Table 1. These models are used to depict the G/G_{max}–γ and D–γ curves under certain conditions. They commonly use a modified hyperbolic model to represent the G reduction backbone curve, and some factors (such as D_{min} or D_{max}) have been introduced to obtain the best possible fit with the target D–γ data. As a result, the existing models are empirical and were developed for specific soil types, strain ranges, and other considerations. Some are limited to the data used in the fitting, and they fail to provide a good fit for others. Furthermore, these models do not directly take into account the variation of G/G_{max}–γ and D–γ with $H(\sigma_m)$, making it impossible to construct a universal model that can be reliably applied to a variety of data sets.

Table 1. Summary of representative G/G_{max}–γ and D–γ function forms.

Function Forms	Data from	Soil Type
$G/G_{max} = 1/(1+\gamma/\gamma_r)$, $\gamma_r = \tau_{max}/G_{max}$, where G_{max} is the maximum shear modulus; γ_r is the reference strain; τ_{max} is the maximum shear stress.	Hardin and Drnevich [19]	Cohesive soil and sand
$D = D_{max}(1 - G/G_{max})$, where D_{max} is the maximum damping ratio.		
$G/G_{max} = 0.5\left[1+\tanh\left(\ln(0.000102/\gamma)^{0.492}\right)\right]\sigma_m{}^{0.272[1-\tanh(\ln(0.000556/\gamma)^{0.4})]}$,	Ishibashi and Zh-ang [20]	Sandy soil
$D = 0.333\left\{0.586(G/G_{max})^2 - 1.547(G/G_{max}) + 1\right\}$.		
$G/G_{max} = 0.5\left[1+\tanh\left(\ln((0.000102+n(\mathrm{PI}))/\gamma)^{0.492}\right)\right] \times \sigma_m{}^{0.272[1-\tanh(\ln(0.000556/\gamma)^{0.4})]e^{-0.145\mathrm{PI}-0.0145\mathrm{PI}^{1.3}}}$, where n(PI) is the function related to the plasticity index of soil.		Plastic soil (Silt and Clay)
$D = 0.333/2 \times \left(1+e^{-0.0145\mathrm{PI}^{1.3}}\right) \times \left\{0.586(G/G_{max})^2 - 1.547(G/G_{max}) + 1\right\}$.		
$G/G_{max} = 1/\left(\left[1+a(\gamma)^b\right]^c\right)$, where a, b, and c are the curvature coefficient.	Borden et al. [21]	Piedmont residual soil (MH, ML, SM-ML, SM)
$D = 20.4(G/G_{max} - 1)^2 + 3.1$.		
$G/G_{max} = 1/\left[1+(\gamma/\gamma_r)^\alpha\right]$, where α is the curvature coefficient.	Stokoe et al. [22] Darendeli [23]	Undisturbed soil (CH, CL, CL-ML, MH, ML, SC, SM, SC-SM, SP, SP-SM, SW-SC, SW-SM)
$D = d \times (G/G_{max})^{0.1} \times D_{Masing} + D_{min}$, where d is the scaling coefficient, D_{min} is the small-strain damping ratio, and D_{Masing} is the modeled masing damping.	Darendeli [23]	
$G/G_{max} = 1/\left[1+(\gamma/\gamma_r)^\alpha\right]\gamma_r = \gamma_{r1}(\sigma_m/P_a)^k$, where γ_r is the reference strain corresponding to the γ value when $G/G_{max} = 0.5$, α is the curvature parameter, γ_{r1} is the reference strain at a mean effective confining stress σ_m of 100 kPa, P_a is the reference stress at 100 kPa, and k is a stress-correction exponent.	Zhang et al. [24]	Quaternary soil Tertiary and older soil Residual/saprolite soil

Table 1. *Cont.*

Function Forms	Data from	Soil Type
$D = D_{min} + 10.6(G/G_{max})^2 - 31.6(G/G_{max}) + 21.0$ Torsional shear test, $D = D_{min} + 9.4(G/G_{max})^2 - 26.5(G/G_{max}) +$ 17.1 Resonant column test, $D_{min} = D_{min1} \times (\sigma_m/P_a)^{-k/2}$, where D_{min1} is the small-strain damping at σ_m of 100 kPa.		

In view of the special conditions of the marine environment and the relative scarcity of dynamic parameters for marine clay, the properties of G and D of marine clay still need to be further investigated. For this purpose, in this study, a series of RC tests were conducted on marine clay in Hangzhou Bay and Bohai Bay, China. The variation characteristics of G and D with soil depth H (reflected as σ_m in the laboratory test conditions) were studied and analyzed. More importantly, an intelligent prediction model based on a back-propagation neural network (BPNN) was developed. This model is universal and is not affected by differences in fitting parameters, it also takes into account the natural variations of the dynamic mechanical characteristics of soil with the value of $H(\sigma_m)$. It can not only accurately predict the values of G and D with various γ and corresponding $H(\sigma_m)$ values, but it also intelligently describes and predicts the G/G_{max}–γ and D–γ curves of marine clay. Accordingly, this study will advance the understanding of the basic dynamic properties of marine clay in Hangzhou Bay and Bohai Bay. The proposed new-intelligent model will be able to deeply excavate, learn and predict the dynamic characteristics of marine clays. Furthermore, experimental studies and proposed models will provide reliable supplementary data for the analysis of soil dynamics and seismic responses in marine engineering.

2. Experimental Measurements

2.1. Materials

This study examined undisturbed marine clay taken from the seabeds of Bohai Bay and Hangzhou Bay at depths ranging from 6.3 m to 70 m. Using an offshore drilling platform, an open thin-walled earth borrower was employed to capture the clay samples from four boreholes at the locations indicated in Figure 1. In the drilling area in Bohai Bay (BH), the seabed topography is slightly undulating, and the seawater depth varies gently with a moderate deepening trend from southwest to northeast and no obvious local undulations. The bottom terrain in the drilling area in Hangzhou Bay (HZ) is relatively flat, and the seawater depth varies widely, sloping slowly from west to east. A total of 27 marine clay samples were used for this study; 17 samples from Bohai Bay were designated BH1 to BH17, while 10 samples from Hangzhou Bay were designated HZ1 to HZ10, respectively. According to the Unified Soil Classification System [25] and laboratory assessments of basic physical qualities, the undisturbed marine clays were classified as lean clay (CL). RC tests were conducted on the marine clays at σ_m values ranging from 43 to 466 kPa, as summarized in Table 2.

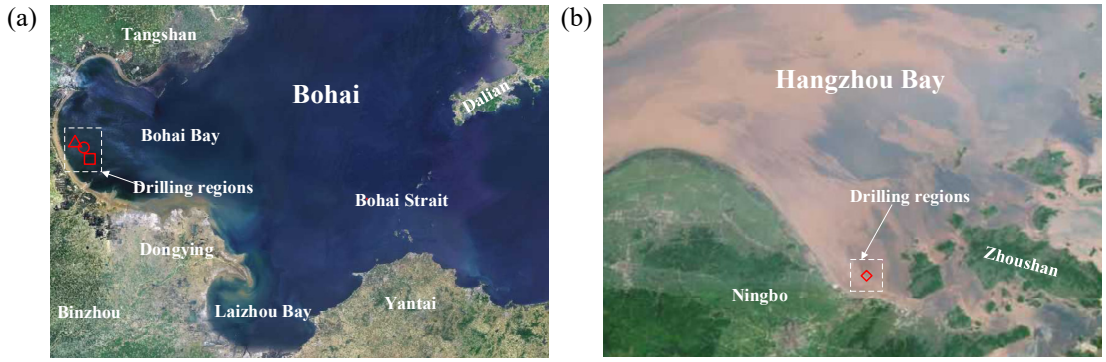

Figure 1. Geographical locations of the boreholes: (**a**) Bohai Bay and (**b**) Hangzhou Bay.

Table 2. Representative physical parameters of the marine clays.

Sample	Soil Depth H/m	Mean Effective Confining Pressure σ_m/kPa	Specific Gravity G_s	Water Content w/%	Density ρ/g·cm^{-3}	Plasticity Index PI
BH 1	6.3–6.5	43	2.67	40.72	1.9	15.99
BH 2	8.3–8.5	56	2.69	36.45	1.9	17.15
BH 3	10.8–11.0	73	2.70	38.95	1.95	16.88
BH 4	15.8–16.0	106	2.68	37.99	1.92	16.23
BH 5	23.5–23.7	157	2.67	37.87	1.97	16.98
BH 6	25.5–25.7	171	2.67	35.53	1.96	16.95
BH 7	29.8–30.0	199	2.67	38.96	1.91	15.00
BH 8	30.0–30.2	201	2.71	36.17	1.97	15.06
BH 9	31.8–32.0	213	2.67	39.04	1.92	17.12
BH 10	33.8–34.0	226	2.68	36.67	1.93	12.64
BH 11	35.2–35.4	235	2.69	36.82	1.93	17.23
BH 12	40.3–40.5	269	2.68	30.93	1.9	15.27
BH 13	43.3–43.5	289	2.70	38.17	1.94	15.95
BH 14	46.3–46.5	309	2.68	36.08	1.93	15.34
BH 15	61.8–62.0	413	2.68	33.74	2.04	13.55
BH 16	67.8–68.0	453	2.68	31.10	1.99	15.57
BH 17	69.8–70.0	466	2.67	30.84	2.01	13.14
HZ 1	18.3–18.5	123	2.68	15.52	1.81	15.52
HZ 2	23.3–25.5	156	2.67	15.64	1.94	15.64
HZ 3	28.3–28.5	190	2.70	14.37	1.97	14.37
HZ 4	33.3–33.5	233	2.67	15.07	2.06	15.07
HZ 5	40.8–41.0	273	2.71	16.57	2.07	16.57
HZ 6	48.3–48.5	323	2.70	14.76	2.07	14.76
HZ 7	53.3–53.5	356	2.69	13.35	2.04	13.35
HZ 8	58.3–58.5	390	2.70	14.76	2.06	14.76
HZ 9	63.3–63.5	423	2.70	15.97	2.06	15.97
HZ 10	68.3–68.5	456	2.69	14.08	2.03	14.08

2.2. Test Apparatus and Procedure

The specimens were tested using the TSH-100 high-precision fixed–free RC apparatus (Figure 2) from GCTS Testing Systems (Tempe, AZ, USA), which can reliably measure the G and D values of soil specimens over a wide strain range with stable and repeatable results. In the device, the confining pressure is controlled by a pneumatic servo system. A fully automatic suspension torsion drive system is used to excite the top of the soil specimen. On-specimen axial displacement can be measured by an AC deformation sensor with a range of ±6 mm and 0.1% linearity, and γ can be measured by a fiber optics deformation sensor with a dual-range output: ±0.1 mm low range and ±5.0 mm for high range, with a 0–15 kHz flat frequency response and 0.1% linearity. The data-acquisition system has eight independent channels with a response frequency of 50 kHz, and it can record data at intervals of less than 0.2 ms.

1 Pressure control panel & volume change device 2 Resonant-column test platform
3 Digital servo controller and acquisition system 4 Computer

Figure 2. Schematic diagram of TSH-100 resonant column apparatus.

The test procedure can be divided into three steps. (1) A solid cylindrical specimen with a diameter of 50 mm and height of 100 mm is mounted on the device base. (2) After the specimen is installed, the top is connected to the floating torsion drive device, the displacement sensor is connected and zeroed, and the pressure chamber is closed to ensure a tight seal. (3) The specimens are uniformly consolidated according to the natural stress state based on the original marine soil depth, as summarized in Table 2. (4) When the average axial-strain rate is less than 1×10^{-3}%/min, the consolidation is completed. The soil specimen is then excited by the automatic suspension dynamic torsion device, and the excitation frequency is steadily increased. (5) Consequently, the value of G is obtained by the theory of elastic-wave propagation once the sweep frequency reaches the resonance frequency, and the value of D is calculated by the collected free-vibration response decay curve [26,27].

$$G = \rho V_S^2 \tag{1}$$

$$\delta = \frac{1}{z}\ln\left(\frac{A_1}{A_{z+1}}\right),\ D = \sqrt{\frac{\delta^2}{4\pi^2+\delta^2}} \times 100\%, \tag{2}$$

where V_S is the shear-wave velocity of the soil [28], δ is the logarithmic decrement of the decay curve, A_1 is the amplitude of free vibration for the first cycle after excitation switch-off, A_{z+1} is the amplitude of free vibration for the $(z + 1)$th cycle of free vibration, and z is the number of free-vibration cycles.

2.3. Experimental Results

The RC test results of the dynamic shear modulus G and damping ratio D versus shear strain γ for marine clay with changes in H (σ_m) are given in Figures 3 and 4, respectively. In line with the phenomena of previous studies, all the marine clays in Bohai Bay and Hangzhou Bay showed exhibited decreases in G and increases in D with increasing γ. Furthermore, it is noteworthy that for a given value of γ, the G value progressively increases with increasing H (σ_m), while D gradually decreases. In addition, based on the hyperbolic relationship between G and γ under small-amplitude vibrations proposed by Hardin and Drnevich [19], a linear relationship between $1/G$ and γ can be obtained, followed by the value of G_{max} for marine clay [29], as illustrated in Figure 5. The G_{max} values of the marine clays also increase with increasing H (σ_m), which is consistent with the experimental findings in Figures 3 and 4. For all the present experimental values, the overall dynamic stiffness decays with increasing γ, but it increases with increasing H (σ_m). This also indicates that the G and D values of marine clay are not only directly related to γ, but they also have an obvious and strong correlation with H (σ_m).

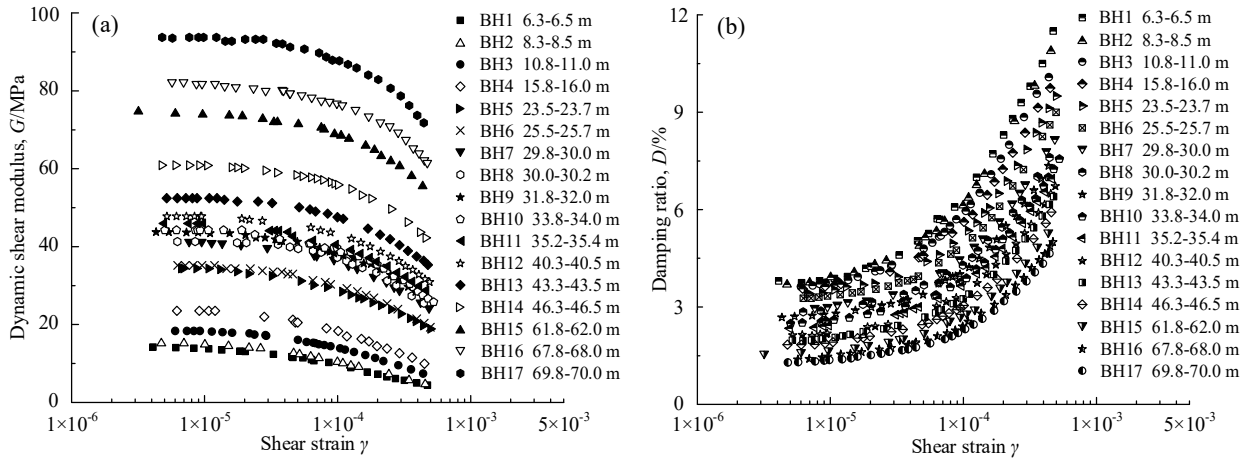

Figure 3. Experimental results of RC tests on marine clay from Bohai Bay: (**a**) variation of dynamic shear modulus with shear strain; (**b**) variation of damping ratio with shear strain.

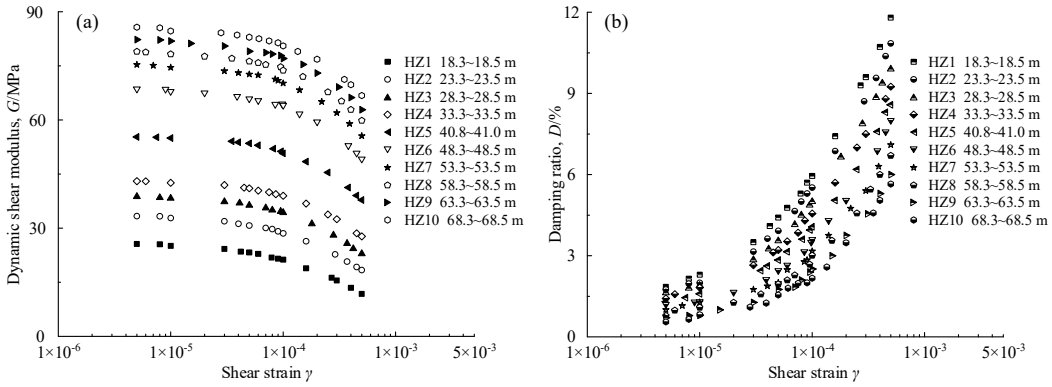

Figure 4. Experimental results of RC tests on marine clay from Hangzhou Bay: (**a**) variation of dynamic shear modulus with shear strain; (**b**) variation of damping ratio with shear strain.

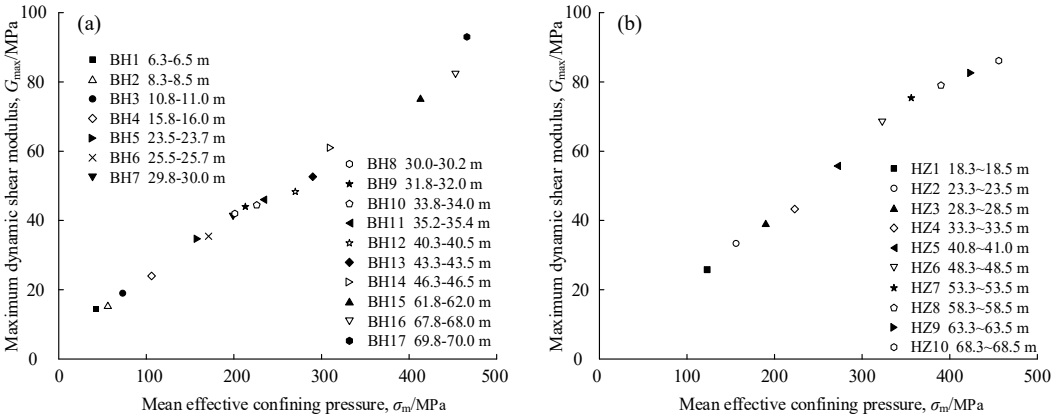

Figure 5. Maximum dynamic shear modulus of marine clays from (**a**) Bohai Bay; (**b**) Hangzhou Bay.

3. Intelligent Model

3.1. Model Framework

The representative and modified hyperbolic models of G/G_{max}–γ normally have more than one curve coefficient for the best fit of the data, as shown in Table 1. In contrast, D–γ models add numerous parameters on the basis of G/G_{max}–γ. In this approach, forward propagation of errors will unavoidably arise in the fitting process of the formula to the application, especially the forward propagation of errors from the G/G_{max}–γ formula to the D–γ formula. To solve this problem, an intelligent model based on a BPNN is proposed. The BPNN proposed by Rumelhart et al. [30] features the forward propagation of data and the back-tpropagation of errors, and it has the ability to self-identify, learn, and model the intrinsic relationships in complex nonlinear data. This makes it particularly suitable for modeling the dynamical behaviors of soil. The intelligent BPNN model framework, which uses the information-processing characteristics of the human brain as the model reference, is shown in Figure 6. Data processing in the BPNN is performed between the input layer (I), the hidden layer (L), and the output layer (O), with each layer consisting of multiple neurons. Each neuron is connected by the weights (W_{ni}) and (W_{jn}), and the neurons (L_n) and (O_j) are controlled by the thresholds (T^H) and (T^O).

3.2. Model Settings and Procedures

The model and algorithm can be described as follows:

(1) Framework: input layer I + hidden layer L + output layer O = 2 + n + 3, as depicted in Figure 6.

(2) Initial process: normalize the data set, and initialize the connection weights and thresholds to 1.

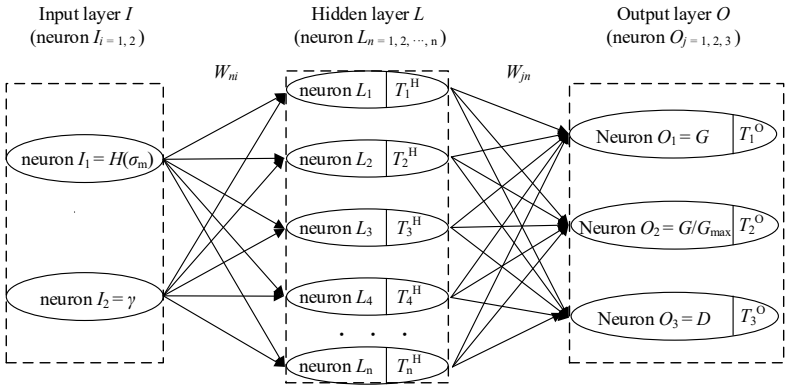

Figure 6. Technical framework for the intelligent model.

(3) Forward propagation: the input data are passed in from I_i, processed by L_n, and then reach O_j. The hyperbolic tangent sigmoid transfer function $f_{\text{Tansig}}(x)$ was chosen as the transfer function from I_i to L_n, and a linear function was chosen as the transfer function from L_n to O_j:

$$L_n = f(\sum_{i=1}^{3} w_{ni} I_i + T_n^H),\ f_{\text{Tansig}}(x) = \frac{1}{1+e^{-2x}} - 1, \tag{3}$$

where x is the input values in the function $f_{\text{Tansig}}(x)$, and

$$O_j = \sum_{n=1}^{n} w_{jn} L_n + T_j^O \tag{4}$$

(4) Back-propagation: if the output value does not match the actual value, it is transferred to the backward-propagation stage of the error. The error is apportioned to all the neurons in each layer and is used as the basis for correcting the weights and thresholds in the training and learning process.

(5) Training and learning: the weights and thresholds are continuously updated using the Bayesian regularization back-propagation and gradient-descent momentum algorithm. According to the Levenberg–Marquardt method [31], the Bayesian regularization back propagation minimizes a linear combination of squared errors and weights so that at the end of the training, the resulting network has good generalization qualities [32]. The gradient-descent momentum algorithm is used to increase the learning rate of weights and thresholds [33]. The principles of these algorithms are not repeated in this paper, and they can be implemented on multiple platforms, including Python, Octave, and MATLAB. The main process of training and learning can be expressed as follows:

$$E = \frac{1}{K}\sum_{1}^{K}|e(k)|^2,\ W_{m+1} = W_m + \eta\frac{\partial E}{\partial W_m},\ T_{m+1} = T_m + \eta\frac{\partial E}{\partial T_m} \tag{5}$$

where $e(k)$ represents the difference between each output value and the training value, E represents the total error, K represents the total number of values in the training set, and m represents the current iteration of the training process.

(6) Finally, when E is reduced to the expected training error, or the number of learning iterations reaches the pre-set maximum, the training of the intelligent model is completed. The trained model can then be applied to the prediction of the dynamic shear modulus G and damping ratio D characteristics of marine soils

3.3. Model Performance

In this study, about 70.7% of the experimental measurements from Bohai Bay and 70.0% of the experimental measurements from Hangzhou Bay were used as training data; this allowed the model to intelligently identify, excavate, and learn the intrinsic G and

D characteristics of the marine clays. The remaining data were used as a prediction set for model validation and error calculation [34]. The number of training trials was set to 1×10^6, the learning rate was set to 10^{-6}, and the training target's minimum error was set to 1×10^{-10}. The total number n of neurons in the hidden layer L was set in the range 3 to 18. No human intervention or additional curvature coefficient setting was required during the process, and machine learning was achieved entirely by the model itself.

The prediction performance of the trained, intelligent model with different n values is shown in Figure 7. It is assessed by the statistical performance indicators obtained by comparing the predicted and measured data in the prediction set. Mean absolute error (MAE), root mean square error (RMSE), and coefficient of correlation (R) were incorporated into the statistical performance indicators to analyze the prediction performance of the model better [35,36]. The MAE of G, G/G_{max}, and D for marine clays are presented in Figure 7a–c, respectively. It is evident that the MAE for marine clays is at a relatively well-desirable level for the intelligent model with different n. In particular, the MAE shows a decreasing trend with the increase in n, and a significant inflection point occurs when n is greater than 6. Subsequently, the MAE fluctuates at a lower level. Moreover, a similar phenomenon is also observed in Figure 7d–f of the RMSE values. Furthermore, the R of the predicted and measured data are presented in Figure 7g–i, where the R is greater than 0.9 for the predicted performance of the intelligent models with different n. It is worth noting that all prediction results correlate well with the measured data, despite the fact that the prediction error fluctuates with n. This further confirms that intelligent models can excavate, learn and predict the G and D values of marine clays. Therefore, the intelligent model has a good prediction performance for the G and D values of the marine clays, and the prediction accuracy does not strictly depend on n. The detailed prediction results of the intelligent model will be further evaluated and discussed in the following section.

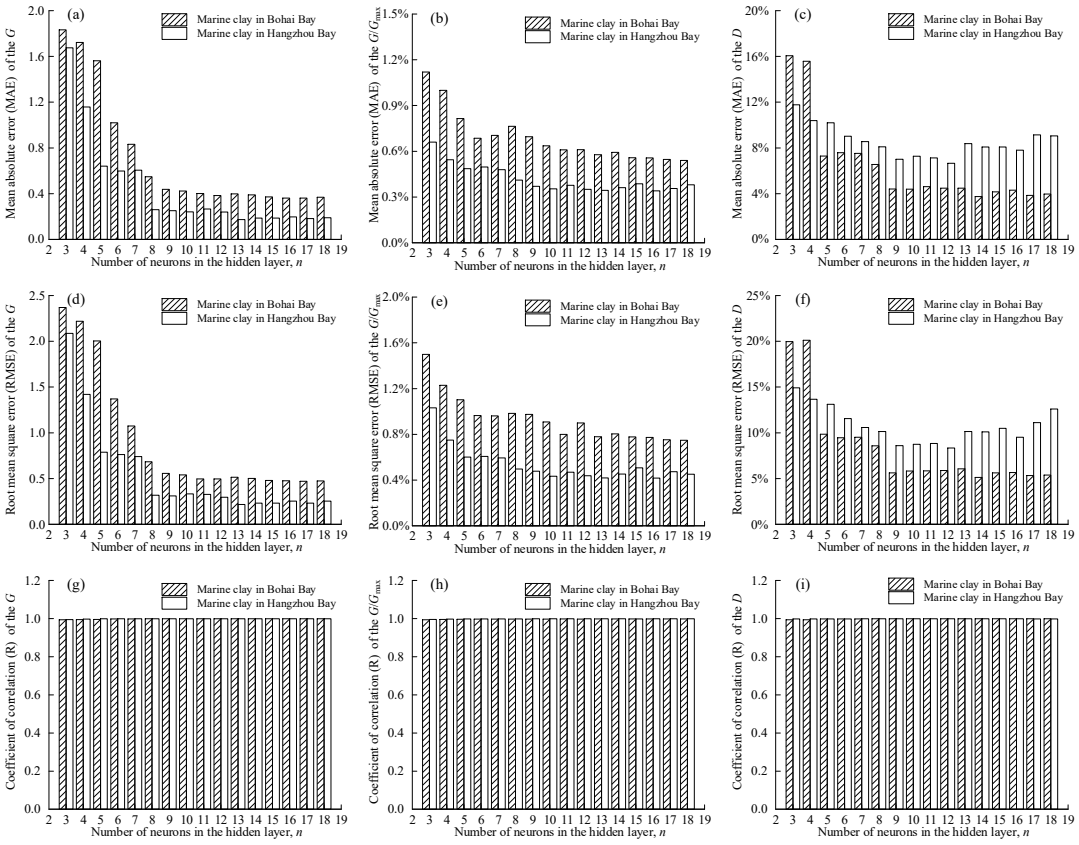

Figure 7. Prediction performance of the intelligent model with different n: (**a**–**c**) the MAE of G, G/G_{max}, and D for marine clays; (**d**–**f**) the RMSE of G, G/G_{max}, and D for marine clays; (**g**–**i**) the R of G, G/G_{max}, and D for marine clays.

4. Evaluation and Discussion

4.1. Evaluation of Prediction Results

To further investigate the effectiveness of the model for identifying, learning, and predicting the dynamic behaviors of marine clay, the values of the prediction set calculated using the intelligent model were compared with the measured data. That is, when both H (σ_m) and γ are known, the prediction effect can be assessed by the difference between the measured value and the predicted value. The results of this comparison are shown in Figures 8 and 9, respectively, with $n = 8$. It can be seen that the relative errors between the predicted and measured values of G and D are generally within ±8%. It should be noted that this error range is quite precise, considering the large uncertainties and complex internal structures of soils.

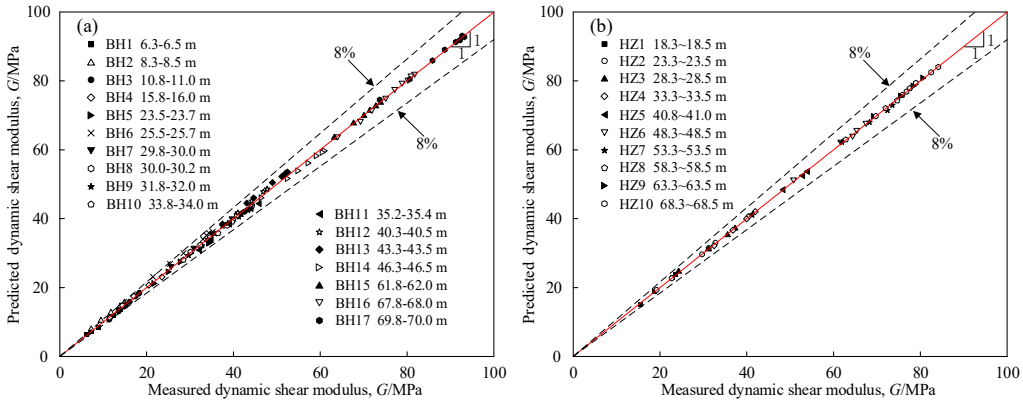

Figure 8. Comparison of predicted and measured values of the dynamic shear modulus G of marine clays from (**a**) Bohai Bay; (**b**) Hangzhou Bay.

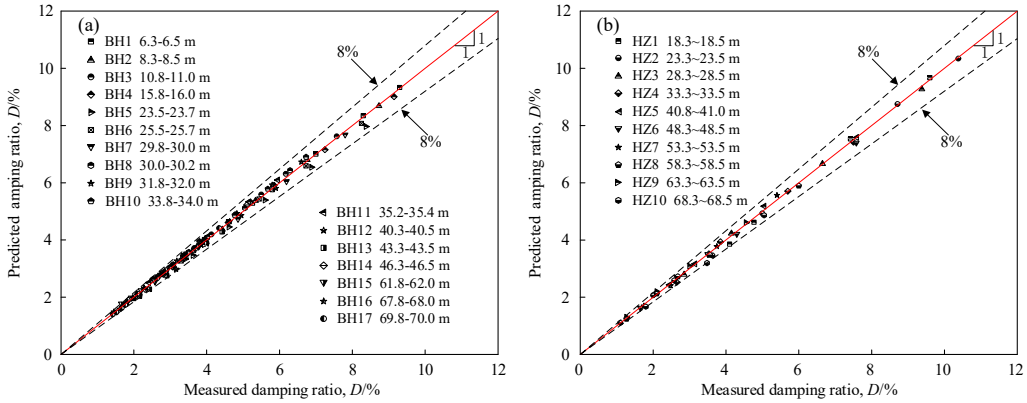

Figure 9. Comparison of predicted and measured values of the damping ratio D of marine clays from (**a**) Bohai Bay; (**b**) Hangzhou Bay.

An important difference between soils and general engineering materials is their nonlinear and hysteretic dynamic behavior. To deeply explore and evaluate the abilities of the intelligent model for prediction of the dynamic properties of marine clay, predicted curves of the normalized dynamic shear modulus G/G_{max} and damping ratio D versus shear strain γ over a wide shear strain range ($1 \times 10^{-6} \leq \gamma \leq 5 \times 10^{-4}$) are presented in Figures 10 and 11, respectively. Combining in Figures 10 and 11, it can be seen that the experimental data are largely in agreement with the predicted curves, and they are also corroborated by the predicted results of G/G_{max} and D in Figures 8 and 9. Specifically, before the line-elastic threshold shear strain ($\gamma_{LE} = 1 \times 10^{-5}$), the G/G_{max} value of marine clay decays slightly with increasing γ, while the value of D increases slightly with increasing γ; when the γ_{LE} is reached, the G/G_{max} value starts to decay at a faster rate with increasing γ, and the value of D increases at a faster rate with increasing γ. Until the nonlinear-

elastic threshold shear strain ($\gamma_{NE} = 1 \times 10^{-4}$) is exceeded, the value of G/G_{max} decays rapidly with increasing γ. Meanwhile, the value of D grows rapidly with increasing γ. Furthermore, the G/G_{max} value increases with increasing H (σ_m) for a given γ value, and this is accompanied by a decreasing recession gradient. Conversely, the D value decreases with increasing H (σ_m) at a given shear strain γ, and this is followed by a decrease in the growth rate.

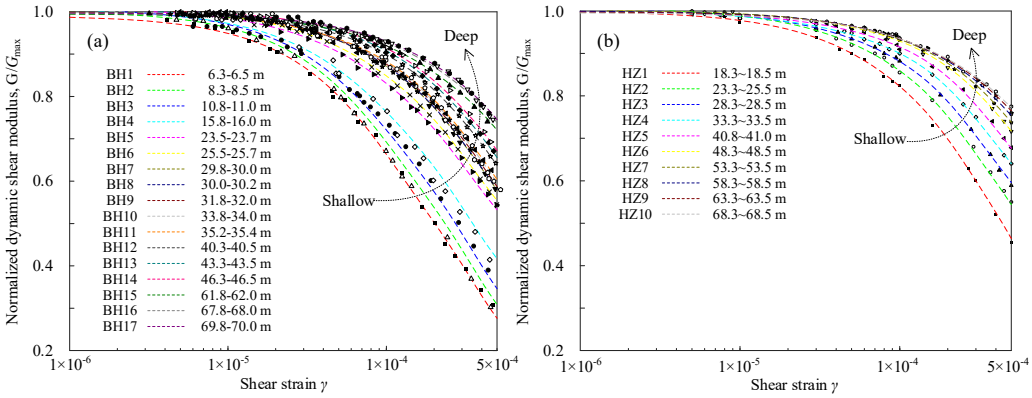

Figure 10. Comparison of measured values and predicted G/G_{max}–γ curves for marine clays from (**a**) Bohai Bay; (**b**) Hangzhou Bay.

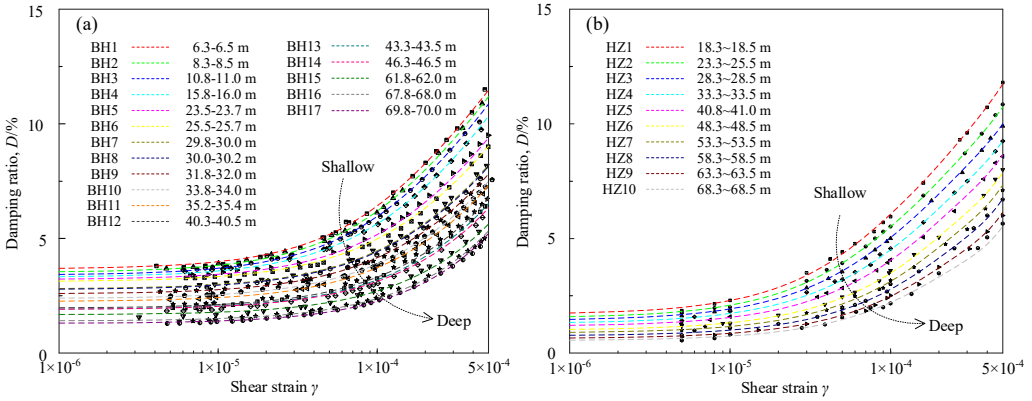

Figure 11. Comparison of measured values and predicted D–γ curves for marine clays from (**a**) Bohai Bay; (**b**) Hangzhou Bay.

In addition, The overall G/G_{max}–γ curves show a "low to high" change tendency; in contrast, the overall D–γ curves show a "high to low" trend. This means that the dynamic properties of the marine clay gradually change from non-linear to linear with increasing H (σ_m), and this is accompanied by weakening hysteresis. Thus, it can be said that the intelligent model can quite effectively describe and predict the nonlinear and hysteretic dynamic properties of marine clay. More importantly, it is not only able to accurately predict the G and D values of marine clays at different H (σ_m) and γ, but it can also intelligently predict the variation of the decay of G and the growth of D with H (σ_m). This will present a solution to a key challenge in geotechnical engineering.

4.2. Comparison with Function Models

It should be noted that most of the formulas in Table 1 do not directly consider the variation of soil dynamic characteristics with H (σ_m), which is an extremely important issue in geotechnical engineering. Hence, the proposed intelligent model was compared with representative mathematical models proposed by Ishibashi and Zhang [20] and Zhang et al. [24] to evaluate its performance. As a control, the evaluation data were used from the prediction set, and the value of n in the model was kept at 8.

Figures 12 and 13 show the performance of the three methods for G/G_{max} and D prediction using the evaluation data. Compared with the mathematical formulas proposed by Ishibashi and Zhang [20] and Zhang et al. [24], the proposed intelligent model has the best performance for the evaluated data. Ishibashi and Zhang's [20] formula overestimates the dynamic stiffness of the soil and is not applicable to marine clay; Zhang et al.'s [24] formula has satisfactory performance for G/G_{max}, but the prediction of D is relatively poor. This is mainly because, to achieve the best fit to the data, their technique normally leads to uncertainty and dispersion of the fitted parameters, and this, in turn, promotes the forward propagation of errors from G/G_{max}–γ to D–γ. Simultaneously, the intrinsic complex nonlinear dynamic characteristics of the marine clay enhance this error-propagation phenomenon. As a result, the proposed intelligent model has a very good match for the G and D properties of the marine clays. Especially for the prediction of D.

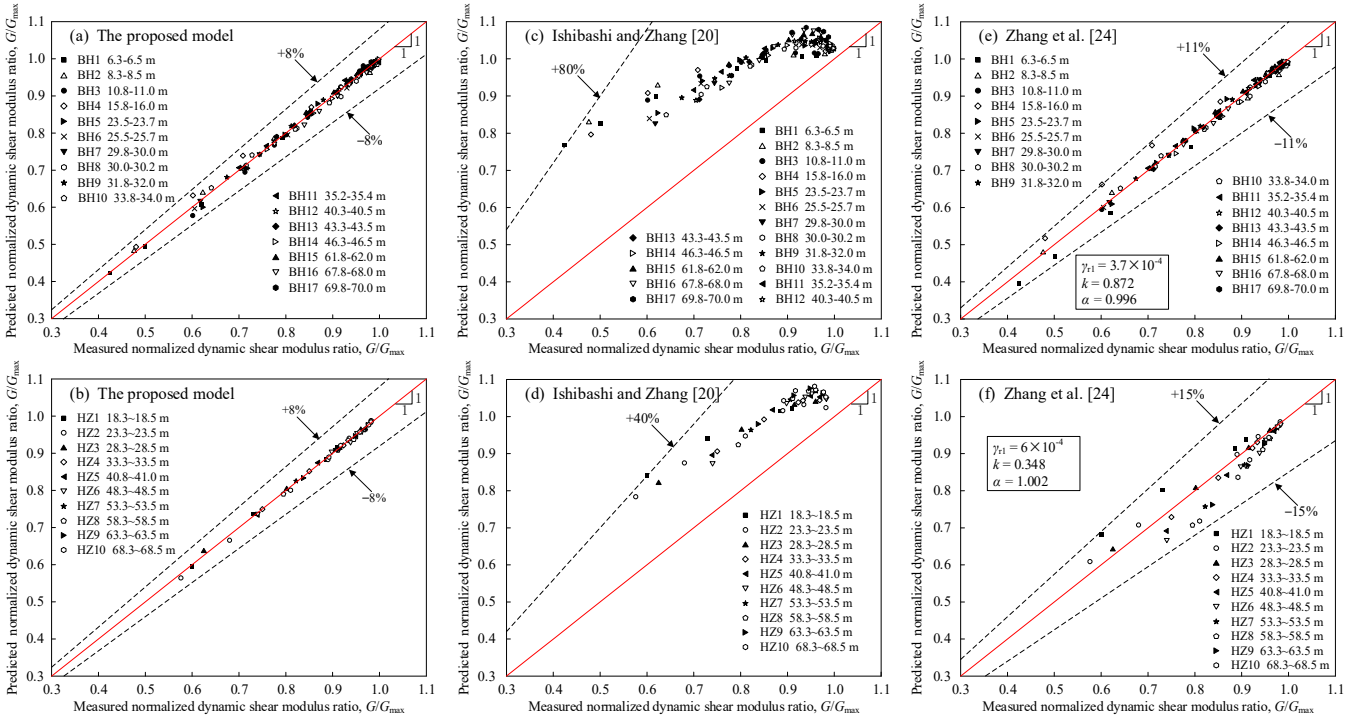

Figure 12. Comparison of the predicted performance of G/G_{max} values: (**a**,**b**) the performance of the proposed model; (**c**,**d**) the performance of the Ishibashi and Zhang's [20] model; (**e**,**f**) the performance of the Zhang et al.'s [24] model.

Thus, compared to the mathematical functions, the proposed intelligent model has very good adaptability to the dynamical characteristics of marine clay from Bohai Bay and Hangzhou Bay, China. This means that it is eminently suitable for application to geotechnical research and earthquake engineering. However, as mentioned before, sampling of the in-situ marine soil is very difficult, especially in different depths. This experimental study and the proposed model in this paper only focus on marine clay in two sea areas. Research on the dynamic properties of undisturbed marine soils is rarely available and still needs to be advanced. More types and locations of marine soils should be studied in further investigation, and an intelligent database should be constructed based on the proposed model.

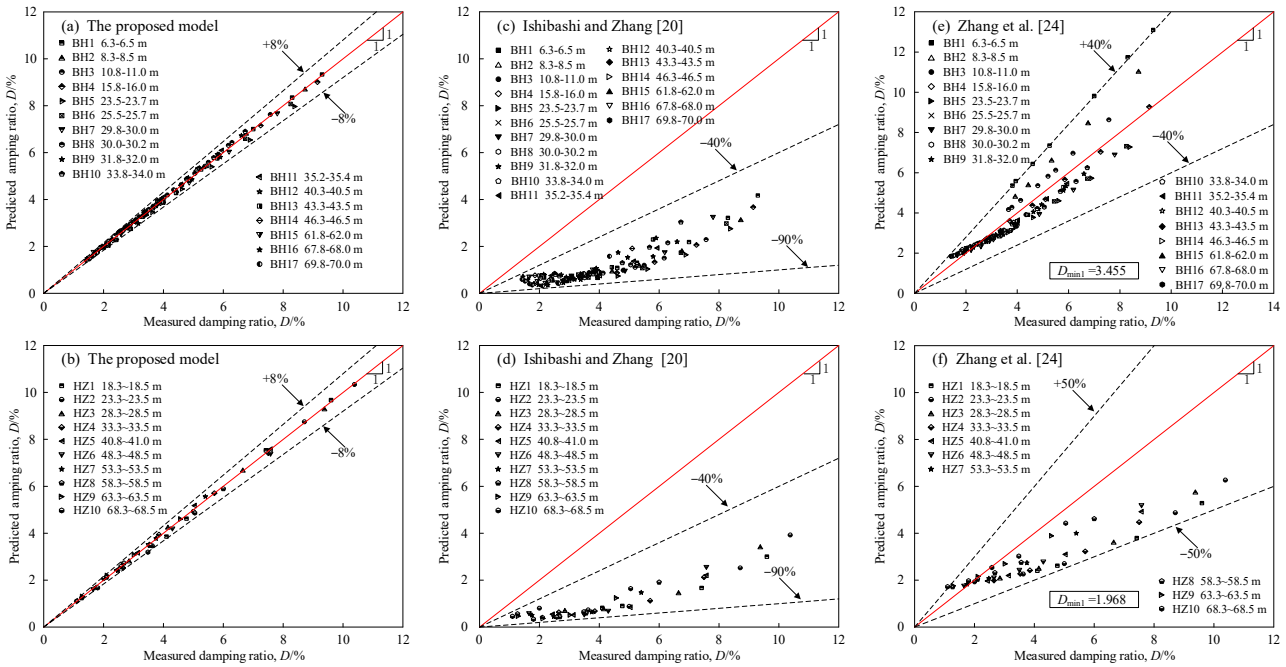

Figure 13. Comparison of the predicted performance of D values: (**a**,**b**) the performance of the proposed model; (**c**,**d**) the performance of the Ishibashi and Zhang's [20] model; (**e**,**f**) the performance of the Zhang et al.'s [24] model.

5. Conclusions

In this study, a series of RC tests were conducted to investigate the variation feature of the G and D with H (σ_m) for marine clays from Bohai Bay and Hangzhou Bay. An intelligent model was constructed that provides a great match for the G and D characteristics of marine clay. The main conclusions can be summarized as follows.

The dynamic properties of marine clays are not only directly related to the γ, but they also have a strong correlation with H (σ_m). The G decay nonlinearly with increasing shear strain γ, and D increases nonlinearly with increasing γ. Meanwhile, the G decay curve G/G_{max}–γ gradually changes from non-linear to linear with increasing H (σ_m), and this is accompanied by a weakening hysteresis in the D growth curve D–γ.

Based on a back-propagation neural network (BPNN), the proposed intelligent model can sufficiently excavate, learn and predict the G and D characteristics of marine clay. It has a good prediction performance for the G, $G/G_{max,}$ and D values of the marine clays with various γ and H (σ_m). Moreover, it can further produce intelligent predictions of the decay of G and the growth of D.

Compared with existing mathematical functions, the intelligent model has a better prediction performance for the G and D properties of the marine clays. It avoids the forward propagation of errors and the need for human intervention regarding the fitting parameters, and the prediction accuracy does not strictly depend on n.

Author Contributions: Conceptualization, Q.W. and W.Y.; methodology, Q.W.; software, Q.W.; validation, Z.W., Y.Q. and W.Y.; investigation, Q.W.; resources, Q.W.; data curation, Z.W.; writing—original draft preparation, Q.W.; writing—review and editing, Q.W. and W.Y.; visualization, Y.Q.; supervision, W.Y.; funding acquisition, Q.W. All authors have read and agreed to the published version of the manuscript.

Funding: This research was funded by the National Natural Science Foundation of China (52008206) and the China Postdoctoral Science Foundation (2021M690279).

Institutional Review Board Statement: Not applicable.

Informed Consent Statement: Not applicable.

Data Availability Statement: The data used during the study are available from the first author by request.

Acknowledgments: Not applicable.

Conflicts of Interest: The authors declare no conflict of interest.

Nomenclature

G = dynamic shear modulus
G_{max} = maximum dynamic shear modulus
G/G_{max} = normalized dynamic shear modulus
D = damping ratio
D_{max} = maximum damping ratio
D_{min} = small-strain damping ratio
γ = shear strain
γ_r = reference strain
τ_{max} = maximum shear stress
a, b, and c = curvature coefficients
α = curvature coefficient
d = scaling coefficient
D_{Masing} = modeled masing damping
H = soil depth
σ_m = mean effective confining pressure
γ_{r1} = reference strain at σ_m of 100 kPa
P_a = reference stress of 100 kPa
k = stress correction exponent
D_{min1} = small-strain damping at σ_m of 100 kPa
w = water content of soil
ρ = density of soil
PI = plasticity index
e = void ratio
δ = logarithmic decrement of the decay curve
V_S = shear wave velocity of soil
A_1 = amplitude of free vibration for the first cycle after excitation switch-off
A_{z+1} = amplitude of free vibration for $(z + 1)^{th}$ cycle of free vibration
z = number of free-vibration cycles in resonant-column test
I = input layer
L = hidden layer
O = output layer
I_i = input layer neurons
L_n = hidden layer neurons
O_j = output layer neurons
i = the number of neurons in the input layer
n = the number of neurons in the hidden layer
j = the number of neurons in the output layer
W_{ni} = connection weights from the input layer to the hidden layer
W_{jn} = connection weights from the hidden layer to the output layer
T^H = thresholds in hidden layer neurons
T^O = output layer neurons
x = input value in function
E = total error
$e(k)$ = difference between each output value and the training value
K = total number of values in the training set
m = current number of the training process
MAE = mean-absolute-error

RMSE = root-mean-square error
R = coefficient of correlation
γ_{LE} = line-elastic threshold shear strain
γ_{NE} = nonlinear-elastic threshold shear strain

References

1. Hardin, B.O.; Drnevich, V.P. Shear modulus and damping in soils: Measurement and parameter effects (Terzaghi Leture). *J. Soil Mech. Found. Div.* **1972**, *98*, 603–624. [CrossRef]
2. Vucetic, M.; Dobry, R. Effect of Soil Plasticity on Cyclic Response. *J. Geotech. Eng.* **1991**, *117*, 89–107. [CrossRef]
3. Chen, G.X.; Zhou, Z.L.; Sun, T.; Wu, Q.; Xu, L.Y.; Khoshnevisan, S.; Ling, D.S. Shear modulus and damping ratio of sand–gravel mixtures over a wide strain range. *J. Earthq. Eng.* **2019**, *23*, 1407–1440. [CrossRef]
4. Yang, W.B.; Wu, Q.; Chen, G.X. Dynamic shear modulus prediction method of undisturbed soil in the estuary of the Yangtze River. *Rock and Soil Mech.* **2019**, *40*, 3889–3996.
5. Morsy, A.M.; Salem, M.A.; Elmamlouk, H.H. Evaluation of dynamic properties of calcareous sands in Egypt at small and medium shear strain ranges. *Soil Dynam. Earthq. Eng.* **2019**, *116*, 692–708. [CrossRef]
6. Jafarian, Y.; Javdanian, H. Small-strain dynamic properties of siliceous-carbonate sand under stress anisotropy. *Soil Dyn. Earthq. Eng.* **2020**, *131*, 106045. [CrossRef]
7. Wu, Q.; Ma, W.J.; Liu, Q.F.; Zhao, K.; Chen, G.X. Dynamic Shear Modulus and Damping Ratio of Rubber-Sand Mixtures with a Wide Range of Rubber Content. *Mater. Today Commun.* **2021**, *27*, 102341. [CrossRef]
8. Upreti, K.; Leong, E.C. Effect of mean grain size on shear modulus degradation and damping ratio curves of sands. *Géotechnique* **2021**, *71*, 205–215. [CrossRef]
9. Wu, Q.; Hang, T.Z.; Zhao, K.; Chen, G.X. Reduction of Dynamic Shear Modulus of Saturated Marine Sandy Silt under Complex Stress Conditions. *Mar. Georesour. Geotechnol.* **2022**, 1–11. [CrossRef]
10. Vrettos, C.; Banzibaganye, G. Effects of specimen size and inertia on resonant column tests applied to sands. *Soil Dyn. Earthq. Eng.* **2022**, *155*, 107136. [CrossRef]
11. Liang, K.; Chen, G.X.; Du, X.L.; Xu, C.S.; Yang, J. A Unified Formula for Small-Strain Shear Modulus of Sandy Soils Based on Extreme Void Ratios. *J. Geotech. Geoenviron. Eng.* **2023**, *149*, 04022127. [CrossRef]
12. Koutsoftas, D.C.; Fisher, J.A. Dynamic properties of two marine clays. *J. Geotech. Geoenviron. Eng.* **1980**, *106*, 645–657. [CrossRef]
13. Vrettos, C.; Savidis, S. Shear modulus and damping for Mediterranean sea clays of medium plasticity. In *Earthquakes Geotechnical Engineering*; e Pinto, P.S., Balkema, A.A., Eds.; CRC Press: Lisboa, Portugal, 1999; pp. 71–76.
14. Sun, T.; Chen, G.X.; Zhou, E.Q.; Li, X.J. Experimental study on dynamic shear modulus and damping ratio of silty clay in deep seabed. *J. Civ. Eng.* **2012**, *45*, 9–14.
15. Sun, T.; Chen, G.X.; Zhou, E.Q.; Li, X.J. Experimental study on dynamic shear modulus ratio and damping ratio of shallow marine soils over 100m in Qiongzhou Strait. *Chin. J. Geotech. Eng.* **2013**, *35*, 375–382.
16. Banerjee, S.; Balaji, P. Effect of anisotropy on cyclic properties of Chennai marine clay. *Int. J. Geosynth. Ground Eng.* **2018**, *4*, 27. [CrossRef]
17. Senapati, S.; Banerjee, S.; Thyagaraj, T. Effect of frequency on cyclic response of marine clay saturated with various pore fluids. *Int. J. Geotech. Eng.* **2021**, *15*, 1155–1164. [CrossRef]
18. Li, Y.Y.; Li, P.; Zhu, S. The study on dynamic shear modulus and damping ratio of marine soils based on dynamic triaxial test. *Mar. Georesour. Geotec.* **2022**, *40*, 473–486. [CrossRef]
19. Hardin, B.O.; Drnevich, V.P. Shear modulus and damping in soils: Design equations and curves. *J. Soil Mech. Found. Div.* **1972**, *98*, 667–692. [CrossRef]
20. Ishibashi, I.; Zhang, X. Unified dynamic shear moduli and damping ratios of sand and clay. *Soils Found.* **1993**, *33*, 182–191. [CrossRef]
21. Borden, R.H.; Shao, L.; Gupta, A. Dynamic properties of Piedmont residual soils. *J. Geotech. Eng.* **1996**, *122*, 813–821. [CrossRef]
22. Stokoe, K.H.; Darendeli, M.B.; Andrus, R.D.; Brown, L.T. Dynamic soil properties: Laboratory, field and correlation studies. In Proceedings of the 2nd International Conference on Earthquake Geotechnical Engineering, Lisbon, Portugal, 21–25 June 1999; pp. 811–845.
23. Darendeli, M. Development of a New Family of Normalized Modulus Reduction and Material Damping Curves. Ph.D. Thesis, University of Texas, Austin, TX, USA, 2001.
24. Zhang, J.; Andrus, R.D.; Juang, C.H. Normalized shear modulus and material damping ratio relationships. *J. Geotech. Geoenviron. Eng.* **2001**, *131*, 453–464. [CrossRef]
25. *ASTM D2487-17*; Standard Practice for Classification of Soils for Engineering Purposes (Unified Soil Classification System). ASTM International: West Conshohocken, PA, USA, 2017.
26. *ASTM D4015-15*; Standard Test Methods for Modulus and Damping of Soils by Fixed-Base Resonant Column Devices. ASTM International: West Conshohocken, PA, USA, 2015.
27. Senetakis, K.; Payan, M. Small strain damping ratio of sands and silty sands subjected to flexural and torsional resonant column excitation. *Soil Dyn. Earthq. Eng.* **2018**, *114*, 448–459. [CrossRef]

28. Chen, G.X.; Wu, Q.; Zhao, K.; Shen, Z.F.; Yang, J. A Binary Packing Material–Based Procedure for Evaluating Soil Liquefaction Triggering during Earthquakes. *J. Geotech. Geoenviron. Eng.* **2020**, *146*, 04020040. [CrossRef]
29. Gao, H.M.; Xia, S.S.; Chen, F.Y.; Stuedlein, A.W.; Li, X.; Wang, Z.H.; Shen, Z.F.; Chen, X.M. Dynamic shear modulus and damping of cemented and uncemented lightweight expanded clay aggregate (LECA) at low strains. *Soil Dyn. Earthq. Eng.* **2021**, *142*, 106555. [CrossRef]
30. Rumelhart, D.E.; Hinton, G.E.; Williams, R.J. Learning representations by back-propagating errors. *Nature* **1986**, *323*, 533–536. [CrossRef]
31. Marquardt, D.W. An algorithm for least-squares estimation of nonlinear parameters. *J. Soc. Ind. Appl. Math.* **1963**, *11*, 431–441. [CrossRef]
32. MacKay, D.J.C. Bayesian interpolation. *Neural Comput.* **1992**, *4*, 415–447. [CrossRef]
33. Qian, N. On the momentum term in gradient descent learning algorithms. *Neural Netw.* **1999**, *12*, 145–151. [CrossRef]
34. Mohammad, A.T.; Mat, S.B.; Sulaiman, M.Y.; Sopian, K.; Al-abidi, A.A. Implementation and Validation of an Artificial Neural Network for Predicting the Performance of a Liquid Desiccant Dehumidifier. *Energy Convers. Manag.* **2013**, *67*, 240–250. [CrossRef]
35. Alzabeebee, S.; Alshkane, Y.M.; Al-Taie, A.J.; Rashed, K.A. Soft Computing of the Recompression Index of Fine-Grained Soils. *Soft Comput.* **2021**, *25*, 15297–15312. [CrossRef]
36. Alzabeebee, S.; Mohammed, D.A.; Alshkane, Y.M. Experimental Study and Soft Computing Modeling of the Unconfined Compressive Strength of Limestone Rocks Considering Dry and Saturation Conditions. *Rock Mech. Rock Eng.* **2022**, *55*, 5535–5554. [CrossRef]